Eur. Phys. J. D **42**, 41–47 (2007)
DOI: 10.1140/epjd/e2006-00275-y

THE EUROPEAN PHYSICAL JOURNAL D

High resolution polarization spectroscopy and laser induced fluorescence of CO_2 around 2 μm

Z.T. Alwahabi[1,a], J. Zetterberg[2], Z.S. Li[2], and M. Aldén[2]

[1] School of Chemical Engineering, University of Adelaide, SA, 5005, Australia
[2] Division of Combustion Physics, Lund University, P.O. Box 118, 221 00 Lund, Sweden

Received 19 September 2006 / Received in final form 21 November 2006
Published online 22 December 2006 –

Abstract. High resolution Infrared Polarisation Spectroscopy (IRPS) and Infrared Laser Induced Fluorescence (IRLIF) techniques were used to probe CO_2/N_2 binary gas mixture at atmospheric pressure and ambient temperature. The probed CO_2 molecules were prepared by laser excitation to an overtone and combination ro-vibrational state (12^01, $J = 15$) of CO_2, centred at 4988.6612 cm^{-1}. IRPS and IRLIF line profiles were recorded for several CO_2/N_2 binary mixtures. The observed IRLIF line shapes have the expected Lorentzian form while the observed IRPS line shapes are narrower by a factor of two than those recorded with the IRLIF and appear to have a Lorentzian-cubed profile. The recorded line profiles provide measurements of the pressure-broadening coefficient directly at atmospheric pressure. The Full-Width-Half-Maxima (FWHM) pressure broadening coefficients are measured, based on IRLIF, to be 0.2174 ± 0.0092 cm^{-1}atm^{-1} and 0.1327 ± 0.0077 cm^{-1}atm^{-1} for self- and N_2 collision broadening, respectively. The broadening coefficients obtained based on IRPS were measured to be ∼8% larger than those obtained with IRLIF.

PACS. 42.25.Ja Polarization – 42.62.Fi Laser spectroscopy – 33.70.Jg Line and band widths, shapes, and shifts

1 Introduction

Quantitative detection of chemical species in the gas phase is an important goal in environmental, industrial, applied and fundamental sciences. Advanced laser diagnostic techniques offer capability for spatially resolved instantaneous chemical species detection. Laser-Induced-Fluorescence (LIF) and laser Polarisation Spectroscopy (PS) have been proven to be very sensitive and offer very good signal to noise ratio. The detected signal is, however, strongly influenced by the self- and foreign-gas collisions, complicating the goal of obtaining quantitative information. LIF and PS are influenced differently by molecular collisions, and this study focus on the effect of collisions on the IRLIF and IRPS line shapes. The detection in the mid infrared offers great advantages, since most molecules possess infrared-active vibrational transitions, with the exception of homonuclear diatomic molecules such as H_2, O_2, and N_2. The IRLIF technique has been a focus of a few recent studies. For example, planar IRLF of CO and CO_2 were reported by Kirby et al., using IR laser radiation around 2.3 μm [1–4]. Webber et al. reported high-resolution absorption measurements of CO_2 in a flat flame burner using a distributed-feedback diode-laser near 2.0 μm [5]. IRLIF of water at 2.7 μm, with IR excitation at 1.39 μm, was reported by Li et al. [6].

The use of IRPS to detect CO_2 molecules in a CO_2/Ar mixture at atmospheric pressure using ∼2.7 μm, was reported by Roy et al. [7], under saturation pump beam condition. Alwahabi et al. reported the use of IRPS at ∼2.0 μm to detect CO_2 in a CO_2/N_2 at room temperature, under the condition of a non saturated pump beam [8]. Li et al., using 3.4 μm, reported the use of IRPS in cold flow and in flames to detect CH_4 [9] and H_2O [10]. In addition, Li et al. have demonstrated very recently that IRPS can also be applied to larger hydrocarbon molecules in cold flows and flames [11,12].

In present paper, we present the measurements of IRLIF and IRPS line shapes of CO_2 (12^01-00^00, R14), recorded at atmospheric pressure and room temperature, for several CO_2–N_2 binary mixtures.

2 Theory

The non saturated IRLIF signal strength, I_{IRLIF}, may be given [13] by,

$$I_{IRLIF} = BI_L\tau_L N f_B \phi F_{IRLIF}(\Omega/4\pi)\varepsilon\eta V \times \int_{\omega} L(\omega')g(\omega)d\omega, \quad (1)$$

[a] e-mail: zeyad.alwahabi@adelaide.edu.au

where B is the Einstein absorption coefficient divided by the speed of light, I_L is the laser spectral power density per unit area divided by the laser bandwidth, τ_L is the laser pulse length, N is the number of CO_2 molecules, f_B the Boltzmann fraction of the CO_2 molecules in the 00^00, $j = 14$ state, ϕ is the IRLIF quantum yield from the excited state, F_{IRLIF} is the fraction of the IRLIF collected within the detector bandwidth, Ω is the solid angle of the IRLIF collected, ε is the transmission of the IR detector, η is the photoelectron efficiency of the combine IR detection system and V is the interaction volume. The integration $\int_\omega L(\omega')g(\omega)d\omega$ reflects the overlap between the laser line profile $L(\omega')$ and the normalized CO_2 absorption profile, $g(\omega)$.

At room temperature, the Doppler line width, $\Delta\omega_{\mathrm{D}}$(FWHM), of the CO_2 R14 line is 0.00917 cm^{-1}, which is more than 20 times smaller than the observed line widths. It is clear that, based on the pressure and temperature conditions in this study, the pressure broadening is dominant, as may be seen later from Figure 2. Therefore the term $g(\omega)$ has the pressure broadened normalized Lorentzian profile, given [14] as,

$$g(\omega) = \frac{1}{1 + \left(2\left(\omega - \omega_0\right) / \left(\Delta\omega_n + \Delta\omega_{self} + \Delta\omega_{foreign}\right)\right)^2}. \tag{2}$$

Here $\Delta\omega_n$ is the natural linewidth, ω is the laser wavelength in cm^{-1}, ω_0 is the central wavelength for the transition, $\Delta\omega_{self}$ and $\Delta\omega_{foreign}$ are the line broadening due the self and the buffer gas collisions, respectively. Combining equations (1) and (2), and ignoring the natural linewidth, as it is much smaller than the collisional broadening, the non saturated IRLIF signal strength as a function of the laser wavelength, $I_{IRLIF}(\omega)$, becomes

$$I_{IRLIF}(\omega_L) \cong BI_L\tau_L N f_B \phi F_{IRLIF}(\Omega/4\pi) \times \varepsilon\eta V \left(\frac{1}{1 + \left(2\left(\omega_L - \omega_0\right) / \left(\Delta\omega_{self} + \Delta\omega_{foreign}\right)\right)^2}\right). \tag{3}$$

A delta function was assumed for the laser profile in the derivative of equation (3).

In contrast to IRLIF, IRPS detects the polarisation change in a weak polarised probe beam due to the passage through a gaseous medium pumped by a strong polarised pump beam. The optical pumping of the target species induces birefringence and dichroism, producing detectable polarisation changes in the weak probe beam. Using two crossed high quality polarisers in the probe beam path, enclosing the region of optical pumping, a small polarisation change in the probe beam can be detected. Both pump and probe beams are tuned to optical transitions of the target species sharing the same lower level. The pump beam may be either linearly or circularly polarised. For the case of a linearly polarised pump beam, typically the probe beam is linearly polarised at $\pi/4$ to the pump beam. Hence it can be described as being composed equally of components parallel and perpendicular to the pump beam polarisation direction. For the case of a circularly polarised pump beam, the linearly polarised probe beam may be equally decomposed into right and left circularly polarised components.

When the polarizers are perfectly crossed and there is no birefringent interference from windows in the pathway of the probe beam, as in the case of this study, the transmitted PS signal, I_{IRPS} can be written [14,15] as

$$I_{IRPS} \cong I_{probe}\left(\xi + \left(\frac{\Delta\alpha L}{4}\right)^2 G(\omega)\right). \tag{4}$$

Here I_{probe} is the input probe beam intensity, ξ is the extinction ratio of the polarizers, L is the length of the interaction volume measured along the probe beam path, $\Delta\alpha$ is the induced dichroism and $G(\omega)$ represents the normalized line shape of the CO_2 absorption function. The concentration of the CO_2 molecules is contained within the induced dichroism term $\Delta\alpha$ [16] as

$$\Delta\alpha = N f_B \sigma^2_{J_f \leftarrow J_i} \frac{I_{pump}\tau_{pump}}{\hbar\omega} \zeta_{J_f \leftarrow J_i}. \tag{5}$$

Here N is the number of CO_2 molecules, f_B the Boltzmann fraction of the CO_2 molecules in the 00^00, $j = 14$ state, $\sigma_{J_f \leftarrow J_i}$ is the absorption cross-section from J initial to J final, I_{pump} is the pump beam intensity, τ_{pump} is the pump beam pulse length and $\zeta_{J_f \leftarrow J_i}$ is a polarization numerical factor listed in reference [16].

When PS was firstly published by Wieman and Hänsch in 1976 [15], it was reported that the PS line shapes are Lorentzian if the Doppler width is greater the collision width. However, Teets et al. [16] and Demtröder [14] assumed that the PS lineshapes are always Lorentzian and outlined the transmitted I_{IRPS}, based on the Lorentzian profile as shown in references [14,16]. After 23 years from the original work of Wieman and Hänsch, Reichardt and Lucht reported theoretical calculation of the PS line shapes in 1998 [17]. They used direct numerical integration of the time-dependent density matrix equation and predicted that, at larger values of the Doppler width and non-saturated pump energy, the PS line shapes do approach the Lorentzian limit. However, at small values of Doppler width and non-saturated pump energy, the PS line shapes are no longer Lorentzian but Lorentzian-cubed.

Based on Reichardt and Lucht [17], equation (2) may be combined with equations (4) and (5), to write the transmitted I_{IRPS} signal for binary mixture as:

$$I_{IRPS}(\omega_L) \cong I_{probe}\left(\xi + \left(\frac{N f_B \sigma^2_{J_f \leftarrow J_i} L I_{pump}\tau_{pump}\zeta_{J_f \leftarrow J_i}}{4\hbar\omega}\right)^2 \times \left(\frac{1}{1 + \left(2\left(\omega_L - \omega_0\right) / \left(\Delta\omega_{self} + \Delta\omega_{foreign}\right)\right)^2}\right)^3\right). \tag{6}$$

Equation (6) describes the non-saturated IRPS signal strength when the pressure broadening is larger than the Doppler broadening and it is suitable for the application of

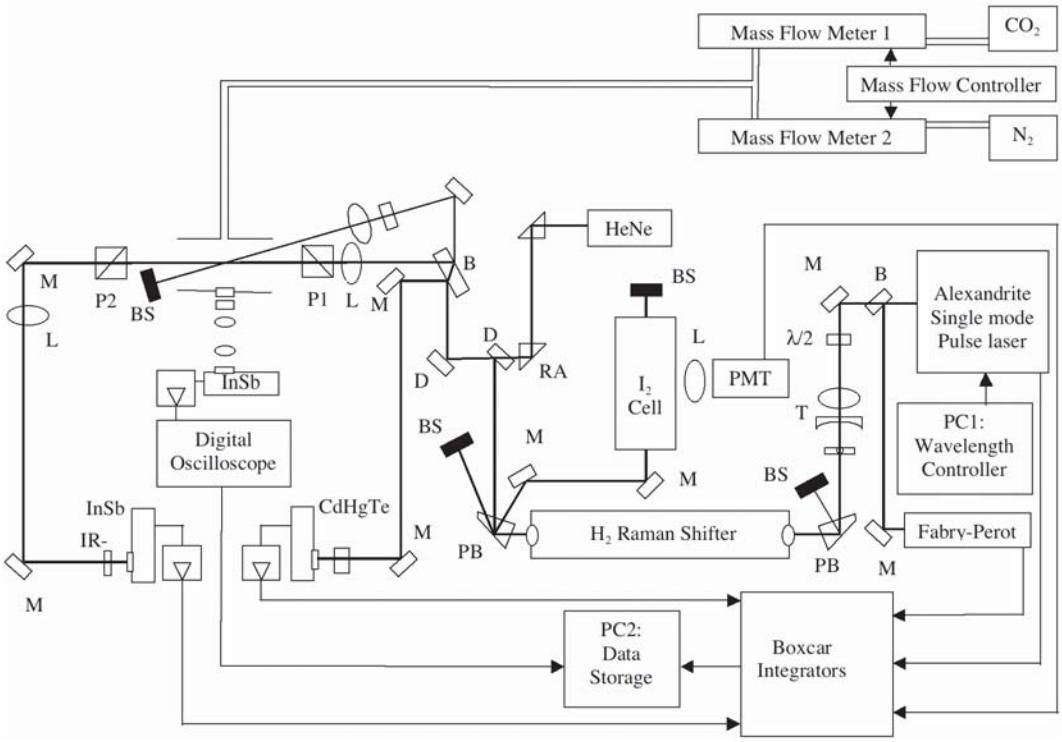

Fig. 1. Schematic diagram of the experimental arrangement. PR, polarization rotator; BS, beam splitter; BC, beam combiner; Ch1, Ch2, signals connected to boxcar channel 1 and channel 2. The optical arrangement for both of IRLIF and IRPS are shown.

IRPS at atmospheric pressure. In the case of Lorentzian-cubed line shapes, it is expected that the signal intensity responds more strongly to the laser frequency than the Lorentzian one. To the author's best knowledge, there has not been any report of a systematic experimental study of PS line shapes under the pressure broadening and non-saturation pump beam energy, the conditions necessary to observe the Lorentzian-cubed profiles outlined in equation (6).

3 Experimental

The optical arrangement is based on an Alexandrite flash-lamp pumped ring cavity laser system (PAL/PRO^{TM}, Light Age Inc.). The fundamental output of the laser continuously covers the spectral range from 739 nm to 785 nm. A tunable, single frequency, external-cavity diode laser (Newport 2020A) is utilized as a seeding source to narrow and continuously scan the output frequency. The laser produces a line width of $\sim$0.002 cm^{-1} at the fundamental, and $\sim$150–200 mJ per pulse with 80–100 ns pulse length. The laser system locks itself to the frequency of the seeded source on a single-shot basis [18]. Based on stimulated Raman scattering, the output laser frequency, in the near IR range, was shifted to the mid IR range by a high pressure cell filled with H_2 gas. The optical arrangement of the IRPS and IRLIF techniques is shown in Figure 1 and a detailed description may be found elsewhere [8]. Briefly, the second Stokes component, centred at around 2 μm, was selected and spatially overlapped with a He–Ne laser beam by a dichroic beam combiner. Visualized by the red He–Ne beam, the infrared beam was then directed to a 8 mm quartz plate. The front reflection, $\sim$4%, of the 2 μm laser radiation was directed to a 77 K CdHgTe infrared detector to monitor the energy of every 2 μm laser pulse. The back reflection, which forms the probe beam, was focused by a spherical lens (f = 600 mm) and set to pass through two fully crossed BBO polarisers. The beam was then reflected by two aluminium mirrors to a 77 K InSb infrared photovoltaic detector (Judson, J10D). The main (pump) beam, was directed to pass through a calcite polariser and then to a variable wave plate and finally to a spherical lens (f = 600 mm). The angle between the probe and the pump beam was set to 7°.

The IRLIF was collected perpendicular to the excitation beam with two CaF_2 spherical lenses (f = 250 mm) and filtered with a narrow band interference filter (centred at 4.27 μm) before being detected by the infrared detector. The LIF signal from the InSb was first amplified in a preamplifier (Judson, PA-9) and then integrated in the boxcar integrator. The data were transferred and stored in a PC for further analysis.

The flow of the CO_2 (AGA, 99.99%) and N_2 (AGA, 99.99%) gases were precisely controlled by two mass-flow meters (Bronkhorst HIGH-TECH). The outlets of two mass flowmeter units were connected to a long Teflon tube of 10 m in length, to ensure complete mixing of the gases. The binary mixture was then introduced to the middle of an open-ended tube of 1 cm in diameter and 5 cm long,

as shown in Figure 1. The system allows the study of any mixing ratio of two gases under a constant atmospheric pressure.

4 Results and discussion

The CO_2 concentration, quantity N in equations (3) and (6), was varied in a CO_2/N_2 binary mixture. Scanning the laser wavelength around the absorption line of the R14 ($12^01 \leftarrow 00^00$) transition, both IRLIF and IRLPS spectra were recorded for several CO_2/N_2 binary mixtures, at ambient temperature and atmospheric pressure. Scans without CO_2 in the sample were also preformed to accurately determine the baseline of the laser excitation spectra. The IRLIF and IRPS were averaged for 8 shots and it was verified that all the measurements in this study were preformed under non-saturation IRPS. The IRLIF and the IRLPS signal were not collected simultaneously.

To obtain the pressure broadening parameters, the IRLIF signal intensity was fitted, with a Lorentzian function, based on the Marquardt algorithm [19,20]. The fitting procedure predicts the IRLIF intensity at the line centre, $I^{\omega_0}_{IRLIF}$, the transition central wavelength ω_0 in cm^{-1} and the fitted FWHM collision width, $\Delta\omega^{fit}_{collision}$.

It was found that the IRLIF line shapes are fitted very well with a Lorentzian function. However, the observed IRPS line shapes, appear to have a stronger dependence on the laser wavelength and could not be fitted with a standard Lorentzian, unlike the case of the IRLIF. In contrast, the IRPS line profiles are fitted well with a Lorentzian-cubed function form. This finding agrees with equation (6), which is based on the theoretical predication of polarisation spectroscopy line shapes reported by Reichardt and Lucht [17]. Meeuwissen et al. [21] observed a similar dependence in the detection of sodium atoms in a welding plasma and a flame using polarisation spectroscopy. The Lorentzian-cubed dependence was also observed by Bultitude et al. [22] in the high-resolution degenerate four-wave-mixing line shapes of OH radicals in flames.

In Figure 2, a typical Lorentzian-cubed fitting of fifty IRPS data points is shown. A Lorentzian function, with the same collisional width as that used in the Lorentzian-cubed function, is also plotted to highlight the difference between them. In addition, Figure 2 shows a Doppler line profile, presented by a Gaussian function, for CO_2 at room temperature, and laser line shape profile. Figure 3 shows high resolution IRLIF and IRPS scans for five different CO_2/N_2 samples. Scans without CO_2 in the sample were also preformed to determine the baseline of the laser excitation spectra. The observed width, $\Delta\omega^{obs}_{PS}$, of the IRPS line profiles, plotted in Figure 3, appear to be half of the observed IRLIF widths, $\Delta\omega^{obs}_{LIF}$. To understand the reason behind this, a general Lorentzian function form with power n is introduced as,

$$I(\omega) = a_0 \left(\frac{1}{1 + \left(2\left(\omega - \omega_0\right) / \left(\Delta\omega^{fit}_{collision} \right) \right)^2} \right)^n . \quad (7)$$

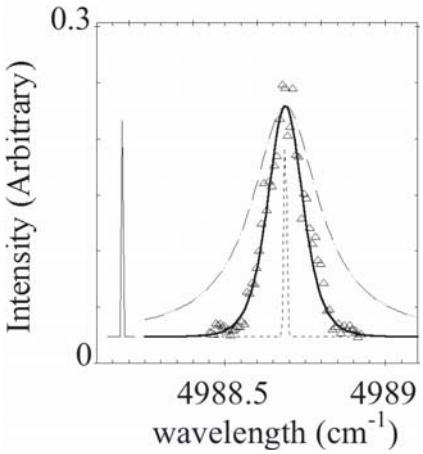

Fig. 2. Illustration of the width and shape of the spectral profiles: a typical Lorentzian-cubed fitting to a typical experimental IRPS data points, solid line; and a Lorentzian function form, dashed line; a Gaussian Doppler profile function of CO_2 with width coefficient of 0.00917 cm^{-1} for the ($12^01 \leftarrow 00^00$) R14 transition at room temperature, dotted line. The sharp peak of the left-hand-side, represents the laser line width. The widths of all profiles are at the correct scale.

By letting $I(\omega) = a_0/2$, where a_0 is the maximum intensity at the line centre, it is easy to show that the general relation between the observed widths, $2(\omega^{I=a_0/2} - \omega_0)$, and the expected collision widths, $\Delta\omega^{fit}_{collision}$, can be written as:

$$2\left(\omega^{I=a_0/2} - \omega_0\right) = \left(2^{\frac{1}{n}} - 1\right)^{\frac{1}{2}} \Delta\omega^{fit}_{collision}. \quad (8)$$

In case of IRLIF, $n = 1$ and therefore the observed IRLIF width, $\Delta\omega^{obs}_{LIF}$, will equal the collisional broadened width, $\Delta\omega^{fit}_{collision}$, as expected. However when $n = 3$, as for the IRPS case, equation (8) becomes,

$$\Delta\omega^{obs}_{PS} = \left(2^{\frac{1}{3}} - 1\right)^{\frac{1}{2}} \Delta\omega^{fit}_{collision}. \quad (9)$$

As the value of $(2^{1/3} - 1)^{1/2}$ approaches 0.5098, the observed IRPS widths appear to be half the expected collisional width, which explains why the IRPS line widths are $\sim$ half of those observed with IRLIF for the same binary mixture, as shown in Figure 3.

As each samples consists of two species, the quantity $\Delta\omega^{fit}_{collision}$ contains the self-collision broadening $\Delta\omega_{CO_2-CO_2}$ and foreign gas collision broadening $\Delta\omega_{CO_2-N_2}$. The widths obtained from the fitting routine are related to the self and foreign gas pressure broadening by $Z_{CO_2-CO_2}$, the number of collisions between CO_2–CO_2, and $Z_{CO_2-N_2}$, the number of collisions between CO_2–N_2, as

$$Z_{total}\Delta\omega^{fit}_{collision} = Z_{CO_2-CO_2}\Delta\omega_{CO_2-CO_2} + Z_{CO_2-N_2}\Delta\omega_{CO_2-N_2}. \quad (10)$$

Here Z_{total} is the total number of collisions.

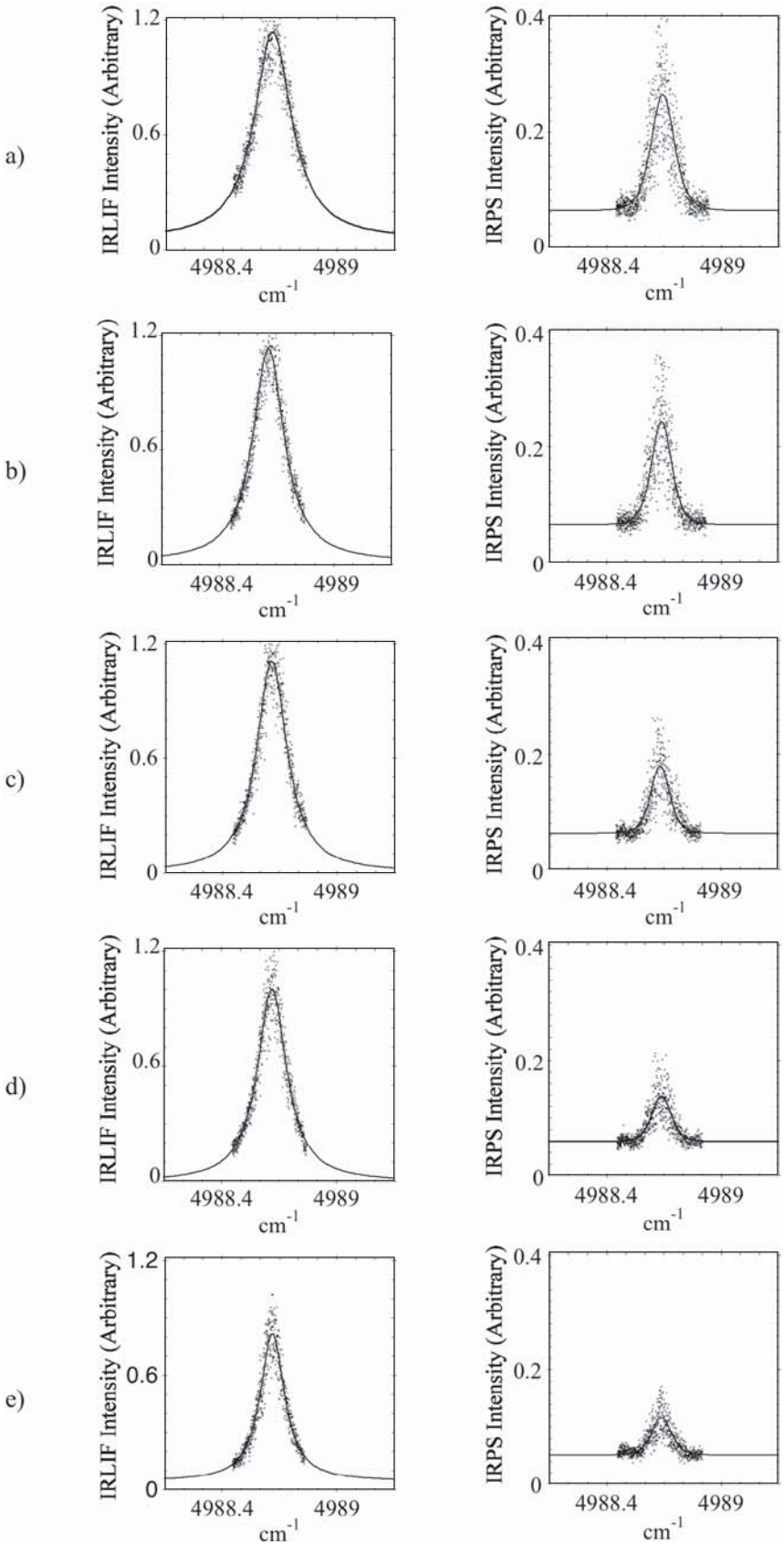

Fig. 3. Typical high-resolution IRLIF and IRPS spectra, shown in dots, for N_2/CO_2 ratios of 0.41, 21.65, 49.70, 76.67 and 177.77 labelled as (a), (b), (c), (d) and (e) respectively. The Lorentzian, in case of IRLIF and Lorentzian-cubed, in case of IRPS, function fits are shown in sold lines.

Table 1. Self- and N_2-pressure broadening coefficients for CO_2 at 295 K. The values of the Lennard-Jones collision rate constant, K_{LJ}, are also listed.

Collider gas	$\Delta\omega_c$ FWHM ($cm^{-1}\,atm^{-1}$)	Rotational Quantum Number J	Ref.	$10^{10}K_{LJ}$ ($cm^3\,molecule^{-1}\,s^{-1}$)
CO_2	0.2174 ± 0.0092	14	This work-IRLIF	3.605
	0.2380 ± 0.0152	14	This work-IRPS	
	0.2260 ± 0.016	14	[25]	
	0.1946	24	[24]	
	0.1744	34	[24]	
N_2	0.1327 ± 0.0077	14	This work-IRLIF	3.444
	0.1407 ± 0.0122	14	This work-IRPS	
	0.1508	24	[24]	
	0.1430	34	[24]	

To obtain $\Delta\omega_{CO_2-CO_2}$ and $\Delta\omega_{CO_2-N_2}$, equation (10) may be rearranged as

$$\left(\frac{1}{f_{CO_2-CO_2}}\right)\Delta\omega^{fit}_{collision} = \Delta\omega_{CO_2-CO_2} + \left(\frac{Z_{CO_2-N_2}}{Z_{CO_2-CO_2}}\right)\Delta\omega_{CO_2-N_2}, \quad (11)$$

where $f_{CO_2-CO_2}$ is the CO_2–CO_2 collision-fraction defined as the number of collisions between CO_2–CO_2 divided by the total number of collisions, Z_{total}.

The number of collisions, Z, was calculated using Lennard-Jones collision rate constant, K_{LJ}, as discussed by Troe [23]. The calculated values of K_{LJ} are listed in Table 1.

The quantity $(\Delta\omega^{fit}_{collision}/f_{CO_2-CO_2})$ was then plotted against $(Z_{CO_2-N_2}/Z_{CO_2-CO_2})$ as shown in Figure 4. A weighted least square linear fitting routine was used to fit the data and the best fitted line is also shown in Figure 4. The intercept and the slope of the fitted line directly represent the $\Delta\omega_{CO_2-CO_2}$ and $\Delta\omega_{CO_2-N_2}$ respectively.

Our measured value of $\Delta\omega_{CO_2-CO_2}$ is 0.2174 ± 0.0092 $cm^{-1}atm^{-1}$ and 0.2380 ± 0.0152 $cm^{-1}atm^{-1}$ obtained from IRLIF and IRPS respectively. Based on IRLIF, the measured value of $\Delta\omega_{CO_2-N_2}$ is 0.1327 ± 0.0077, which is smaller than the 0.1407 ± 0.0122 value measured by the IRPS. The self-collision broadening $\Delta\omega_{CO_2-CO_2}$, and the N_2 collision broadening, $\Delta\omega_{CO_2-N_2}$ for the rotational quantum number $J = 14$ line and listed in Table 1. Our measured pressure broadening values have an error in the range of 4–8%, which was reported by the line-width fitting routine and linear fitting procedures. The measured value of the collision broadening based on the IRPS are ∼1.09 times larger that those measured with IRPLF for the same collision pair, as shown in Figure 4.

It might be argued that the pressure broadening coefficient measured from the IRLIF and IRPS are the same within the experimental (and fitting) error range of ∼4-8%. However, in the light of Figure 4, it seems that the pressure broadening coefficients obtained from the IRPS are always ∼7–9% larger than those obtained by the IRLIF for the same collision pair. This may be due to the fact that we used a focused pump beam in the IRPS study to obtain a reasonable signal to noise ratio for the IRPS signal which is ∼8 times weaker than the IRLIF signal. One reason behind the weak IRPS signal is the very small absorption cross-section, of the $(12^01\text{-}00^00)$ $\sigma_{15\leftarrow14}$ transition, which is ∼1000 times weaker than the fundamental $(00^01\text{-}00^00)$ $\sigma_{15\leftarrow14}$ transition. As the IRPS signal strength scales with the power four of $\sigma_{J_f\leftarrow J_i}$, the IRPS signal is much weaker than the IRLIF signal. For this reason the IRLIF has a higher signal to background ratio of ∼60 compared to ∼8 for IRPS. We conclude, therefore, that the small differences observed from the two different techniques might be due to a very weak power broadening process, which may slightly influence the line profile recorded using IRPS.

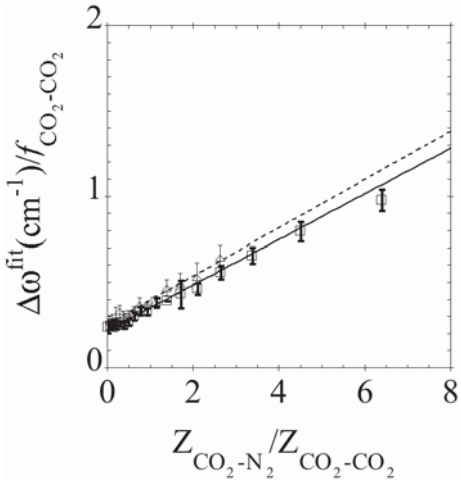

Fig. 4. Pressure broadened fitting parameter, $\Delta\omega^{fit}_{CO_2-N_2}$ versa the ratio of $Z_{CO_2-CO_2}$ over $Z_{CO_2-N_2}$ plot. $\Delta\omega^{fit}_{CO_2-N_2}$ based on IRLIF and IRPS are denoted by (□) and (△), respectively. The error bars are three times the error values reported by the line shapes fitting routine. The weighted leased square linear fitting for the IRLIF and IRPS are presented by sold and dashed lines respectively.

There has been strong interest in the measurements of the pressure broadening coefficients of CO_2 in the $\sim$2 μm spectrum range, as it is important for laser sensing [25–27]. These studies are based on the use of high-resolution absorption spectroscopy. Although absorption spectroscopy offers high resolution in term of wavelength, it lacks the control of the high pressure needed for the measurements of pressure broadening coefficients, especially for the self-broadening. This is because when CO_2 is used at pressure above $\sim$2 Torr the absorption features are saturated even for intra-cavity detection [26]. Therefore, it has been normal practice to measure the self-broadening coefficient at lower pressure and scale the values up.

Using diode laser Absorption Spectra (AS), Corsi et al. reported a measurement of CO_2 self-collision broadening and collisional broadening with N_2 from $j = 22$ to $j = 44$ [24]. Their (FWHM) $\Delta\omega_{CO_2-CO_2}$ vales were 0.1946 cm^{-1} and 0.1744 cm^{-1} for $j = 24$ and $j = 34$, respectively, which shows a very weak inverse dependence on the rotational quantum number J. Our values of $\Delta\omega_{CO_2-CO_2}$, for $J = 14$, is slightly larger than the values obtained by Corsi et al. for $J = 22-44$ as expected. Furthermore, Valero et al. [25] reported a measured value of $\Delta\omega_{CO_2-CO_2}$ of 0.2260 for $J = 14$. Our values of $0.2174\pm0.0092\,cm^{-1}$ and $0.2380\pm0.0092\,cm^{-1}$ agree exceptionally well with Valero et al. values. Our measured value of for $\Delta\omega_{CO_2-N_2}$ ($J = 14$) is 0.1327 ± 0.0077 cm^{-1} and 0.1407 ± 0.0122 cm^{-1} using IRLIF and IRLPS respectively. These values agrees very well with the value of 0.1508 cm^{-1} and 0.1430 cm^{-1}, for $J = 24$ and $J = 34$ respectively, reported by Corsi et al.

5 Conclusions

This work represents the first experimental observation of polarisation spectroscopy line shapes under pressure broadening and non-saturation conditions. High-resolution IRLIF and IRPS spectra for binary mixtures of CO_2–N_2 were recorded using a single-mode, pulsed Alexandrite laser system. It was found that all the recorded IRPS line shapes are Lorentzian-cubed as predicted by Reichardt and Lucht [17] and not Lorentzian as assumed by Teets et al. [16] and Demtröder [14]. The self- and N_2-pressure broadening coefficients were calculated from the recorded line shapes at 760 Torr. Our measured values of $\Delta\omega_{CO_2-CO_2}$ agree exceptionally well with the reported values by Corsi et al. [24] and Valero et al. [25]. However, our measured value of $\Delta\omega_{CO_2-N_2}$ for $j = 14$, is 6% smaller than that reported by Corsi for line $j = 24$. The measured collision broadening values using IRPS are on average $\sim$1.09 larger than those measured with the IRPLF for the same mixture, which might be due to a very weak power broadening process. The techniques presented facilitates the measurement of the self-broadened coefficient directly at atmospheric pressure.

The work was supported by the Swedish Research Council and the Swedish Energy Administration. The first author would like to thank the University of Adelaide for the support through the study leave program.

References

1. B.J. Kirby, R.K. Hanson, Appl. Phys. B **69**, 505 (1999)
2. B.J. Kirby, R.K. Hanson, Proc. Combust. Inst. **28**, 253 (2000)
3. B.J. Kirby, R.K. Hanson, Appl. Opt. **40**, 6136 (2001)
4. B.J. Kirby, R.K. Hanson, Appl. Opt. **41**, 1190 (2002)
5. M.E. Webbe, S. Kim, S.T. Sanders, D.S. Baer, R.K. Hanson, Y. Ikeda, Appl. Opt. **40**, 821 (2001)
6. H. Li, R.K. Hanson, J.B. Jeffries, Meas. Sci Technol. **15**, 1285 (2004)
7. S. Roy, R.P. Lucht, A. Mcilroy, Appl. Phys. B **75**, 875 (2002)
8. Z.T. Alwahabi, Z.S. Li, J. Zetterberg, M. Aldén, Opt. Comm. **233**, 372 (2004)
9. Z.S. Li, M. Rupinski, J. Zetterberg, Z.T. Alwahabi, M. Aldén, Appl. Phys. B **79**, 135 (2004)
10. Z.S. Li, M Rupinski, J. Zetterberg, Z.T. Alwahabi, M. Aldén, Chem. Phys. Lett. **407**, 243 (2005)
11. Z.S. Li, M. Rupinski, J. Zetterberg, M. Aldén, Proc. Combust. Inst. **30**, 1629 (2005)
12. Z.S. Li, M. Levin, J. Zetterberg, J. Kiefer, M. Aldén, Proc. Combust. Inst. **31**, (to appear, 2007)
13. K.C. Smyth, D.R. Crosley, *Applied Combustion Diagnostics*, edited by K. Kohse-Hoighaus, J.B. Jeffries, Taylor (Francis, UK, 2002)
14. W. Demtröder, *Laser Spectroscopy: Basic concepts and instrumentation*, 2nd edn. (Springer-Verlag, Berlin, 1996)
15. C. Wieman, T.W. Hänsch, Phys. Rev. Lett. **36**, 1170 (1976)
16. R.E. Teets, F.V. Kowalski, W.T. Hill, T.N. Carlson, T.W. Hänsch, Proc. Soc. Photo-Opt. Instrum. Eng. **113**, 80 (1977), *Advances in Laser Spectroscopy I*, edited by A.H. Zewail
17. T. Reichardt, R. Lucht, J. Chem. Phys. **109**, 5830 (1998)
18. Z.S. Li, M. Afzelius, J. Zetterberg, M. Aldén, Rev. Sci. Insturm. **75**, 3208 (2004)
19. D.W. Marquardt, J. Soc. Indust. Appl. Math. **11**, 431 (1963).
20. W.H. Press, B.P. Flannery, S.A. Teukolskyand, W.T. Vetterling, *Numerical Recipes in C* (Cambridge University Press, New York, 1988)
21. K. Meeuwissen, O. Lucas, Z.T. Alwahabi, V. Linton, Appl. Spectrosc. (submitted)
22. M. Bultitude, R. Stevens, P. Ewart, Appl. Phys. B **79**, 767 (2004)
23. J. Troe, J. Chem, Phys. **66**, 2758 (1977)
24. C. Corsi, F.D. Amato, M. De Rosa, G. Modugno, Eur. Phys. J. D **6**, 327 (1999)
25. F.P.J. Valero, C.B. Suarez, R.W. Boese, J. Quant. Spectrosc. Radiat Transfer **23**, 337 (1980)
26. J. Geng, J.I. Lunine, G.H. Atkinson, Appl. Opt. **40**, 2551 (2001)